Electronic Transport Properties of Assembled Carbon Nanoribbons

Eduardo Costa Girão,[†,‡] Eduardo Cruz-Silva,[¶,§] and Vincent Meunier*[,§]

[†]Departamento de Física, Universidade Federal do Piauí, CEP 64049-550, Teresina, Piauí, Brazil, [‡]Departamento de Física, Universidade Federal do Ceará, P.O. Box 6030, CEP 60455-900, Fortaleza, Ceará, Brazil, [¶]Department of Polymer Science and Engineering, University of Massachusetts, Amherst, Massachusetts 01003, United States, and [§]Department of Physics, Applied Physics, and Astronomy, Rensselaer Polytechnic Institute, Troy, New York 12180, United States

ABSTRACT

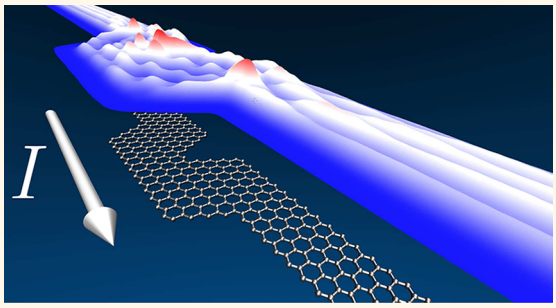

Graphitic nanowiggles (GNWs) are 1D systems with segmented graphitic nanoribbon GNR edges of varying chiralities. They are characterized by the presence of a number of possible different spin distributions along their edges and by electronic band-gaps that are highly sensitive to the details of their geometry. These two properties promote these experimentally observed carbon nanostructures as some of the most promising candidates for developing high-performance nanodevices. Here, we highlight this potential with a detailed understanding of the electronic processes leading to their unique spin-state dependent electronic quantum transport properties. The three classes of GNWs containing at least one zigzag edge (necessary to the observation of multiple-magnetic states) are considered in two distinct geometries: a perfectly periodic system and in a one-GNW-cell system sandwiched between two semi-infinite terminals made up of straight GNRs. The present calculations establish a number of elementary rules to relate fundamental electronic transport functionality, electronic energy, the system geometry, and spin state.

KEYWORDS: graphene nanowiggles · quantum transport · Green's function

Graphene has attracted significant attention since its first isolation as a single sheet.[1] The huge impact of this achievement on nanoscience is in large part due to its potential for graphene-based nanoelectronics as a prospective alternative to silicon electronics.[2,3] Because graphene is a zero-gap semiconductor at zero temperature, it needs to be modified to be useful to a number of applications in electronics demanding a clear electronic band gap.[2] While chemical doping[4] and the random[5−7] or highly ordered[8−10] distribution of structural defects allow for significant changes in graphene's electronic structure, another common approach to manipulate graphene's physical properties is the assembling of 1D graphene substructures by confining the honeycomb lattice in one direction.[11−13] For example, controlling band gap in graphene can be achieved *via* the confinement of the electronic wave function in one-dimension by creating carbon nanotubes or, more directly, carbon nanoribbons (GNRs). GNRs' band gap and magnetic structure depend on the details of the width and edge geometry, and can, in principle, be tuned for a targeted functionality. While a general nanoribbon presents a band gap closely related to its width,[12] the zigzag case (Z-GNRs) is characterized by magnetic ordering along the edges.[13−16] The spins along a single zigzag edge have a ferromagnetic alignment with a magnitude decaying exponentially when moving away from the edges.[13] The edge-to-edge relative alignment can be either ferromagnetic (FM) or antiferromagnetic (AFM) depending whether atoms of opposite edges belong to the same sublattice or not.[17,18] While edge atoms from opposite sides of a straight Z-GNR (such as those studied in ref 13) are in different sublattices (favoring an AFM arrangement), nonparallel edges can belong to the same sublattice (examples can be seen in refs 17−19) leading to a FM edge-to-edge alignment. In addition Z-GNRs are predicted to behave as half-metals.[11]

A number of theoretical investigations have predicted many intriguing physical properties for graphene-like systems.[17,19−23] At the same time, advances in the controlled synthesis of pristine and narrow systems has progressed at a sustained pace.[2,24] Unfortunately, many approaches devised to create single GNR-based devices suffer of a scalability problem since each individual system has to be assembled one-at-a-time. In contrast,

* Address correspondence to meuniv@rpi.edu.

Received for review May 22, 2012 and accepted June 26, 2012.

Published online June 26, 2012
10.1021/nn302259f

bottom-up approaches based on preprogrammed, surface-assisted reactions are able to produce bulk quantities of identical narrow, defect-free, and highly ordered carbon nanostructures in an extremely selective process.[24] The choice of different molecular precursors determines all the details of the resulting carbon nanostructures. To-date, structures realized with this method include three-rings-wide A-GNRs, multiterminal junctions, and complex assembled ribbons with an alternated sequence of short straight edges with either a parallel or oblique arrangement relative to its periodic direction.[24]

It has been argued that this particular segmented structure can be viewed as just an example of a more general set of structures called graphene-nanowiggles (GNWs).[18] The name of this newly synthesized structure originates from the general, wiggle-like, configuration resulting from the periodic arrangements of achiral GNRs at a regular angle. Because the individual sectors are characterized by the relative geometries of a pair of zigzag and/or armchair edges, GNWs can come up in a series of well-defined shapes, namely AA, AZ, ZA, or ZZ (see Figure 1). The electronic and structural properties of these systems,[18,25] as well as the thermoelectric transport properties of a number of them,[26,27] have recently been studied using an array of computational techniques. GNWs with at least one zigzag sector are characterized by a broad diversity of magnetic states compared to Z-GNRs. While ZA-GNWs have a set of states analogous to Z-GNRs, AZ- and ZZ-GNWs are found in up to four different spin-polarized states. This property could be exploited for the development of a series of nanodevices with spin-dependent properties. Critical to their uses in actual devices are their electronic transport properties. These are likely to be noticeably different from GNRs, since GNWs can be seen as a collection of regularly arranged junctions between GNRs of different types. In addition, the presence of spatial domains with varying electronic properties can lead to the appearance of quasi-localized states, which, depending on the system size, can induce size-dependent tunneling across the system.

In this letter, we examine the spin-dependent electronic transport properties of the three classes of GNWs with at least one zigzag edge in two particular configurations. First, we consider the case of a perfect periodic GNW structure. Second, we evaluate the transport characteristics of a single GNW cell sandwiched between two GNRs that serve as electrodes. We discuss the results with emphasis on studying electronic conductance as a function of the electronic energy. Such an approach provides insight into the transport problem within a scattering framework where we compute the quantum transmission probability for electrons with a given energy to tunnel through a device.[28] The association of this transmission with the conductance is the essence of the Landauer formalism employed here.[29,30] Furthermore, quantitative analysis of very low-bias current can be obtained using approximate in-equilibrium equations provided in the Methods section.

RESULTS AND DISCUSSION

The interplay between armchair and zigzag edges in graphitic systems has been shown to result in transport properties which are directly influenced by the spin distribution along the zigzag edges of the structure.[17,19,22] These properties include spin-filter[19] and -valve[17] mechanisms and large magneto-resistance values.[22] Here we show that such interplay, known to be responsible for the diversity of GNWs' spin states, also produces magnetic-state-dependent transport properties of particular importance, especially for potential spintronic applications.

Even though the atomic structure of a given GNW can be obtained from a reduced set of parameters,[25] the geometry of the GNWs is significantly more complex than that of a GNR. This results in a broader and more diverse set of systems for GNWs in comparison with GNRs. As demonstrated recently, the electronic structure of GNWs has a nontrivial dependence on the system's atomic structure.[18,25] Here we choose three particular systems to illustrate the transport properties of this class of structures. This choice is guided by the properties of specific magnetic states. While a semiconductor AFM spin distribution is the ground state for a GNW containing zigzag edges, the other spin-polarized distributions can behave either as a metal or a semiconductor system. The FM distribution is, in particular, special in comparison with most of the other magnetic states as it presents a nonspin degenerate set of energy levels, leading to the possibility of controlling the current flow across GNW-based devices by the choice of the electronic spin. Given the specificity of the FM state, we choose systems where the electronic energy bands for the periodic case in this state present different behaviors around the Fermi energy: one metallic (AZ-GNW) and two semiconductors with one having the highest occupied bands corresponding to majority spin (ZA-GNW) and the other with these bands corresponding to the minority spin (ZZ-GNW). In the following we discuss the results for each case.

AZ-GNWs—Tuning the Gap. We will first consider the case of periodic AZ-GNWs, focusing on the $(11_A,6_Z)$ structure. Details on the terminology employed to classify GNWs have been presented previously.[18,25] Within the TBU approach, this AZ-GNW presents four possible magnetic states, namely antiferromagnetic (AFM), ferromagnetic (FM), linear-antiferromagnetic (LAFM), and trans-antiferromagnetic (TAFM) in addition to the nonmagnetic case (PM).[18] The results of the transport calculations are shown on the left of Figure 2. Quantum conductance for spin-up levels is plotted as a function of the energy around the Fermi energy ($E_F = 0$)

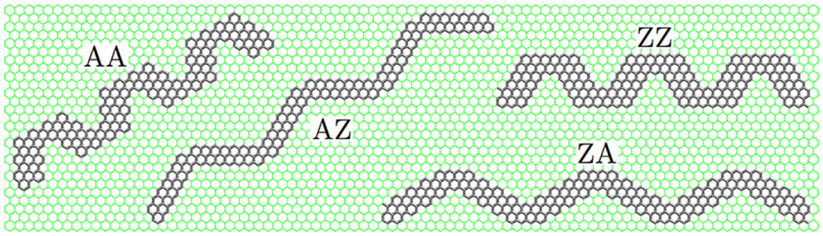

Figure 1. The four classes of achiral GNWs: AA, AZ, ZA, and ZZ, depending on when the parallel and oblique sectors, respectively, present either an armchair (A) or zigzag (Z) edge.

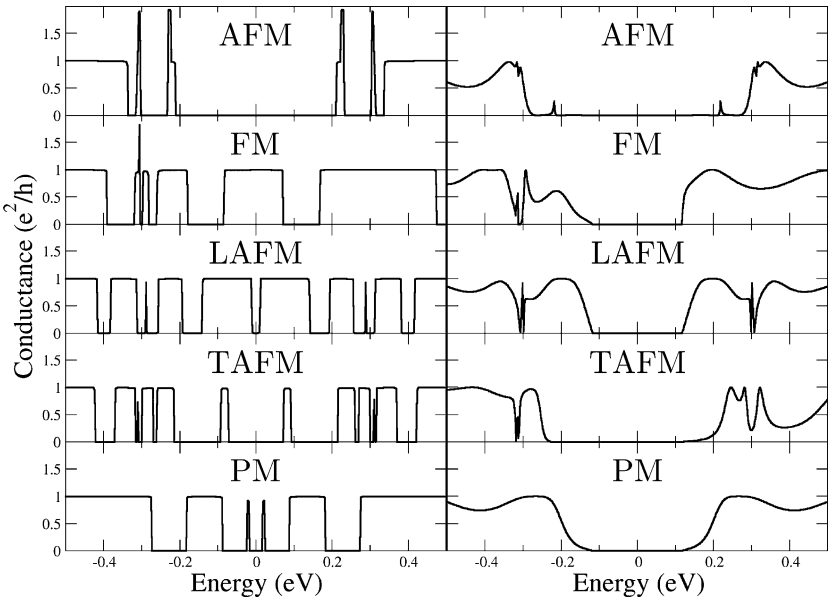

Figure 2. Computed electronic conductance as a function of energy for the spin-up levels in the five possible spin distributions for the (11_A,6_Z) AZ-GNW structure in the periodic (left) and one-cell connected to straight GNRs (right) cases. The corresponding curves for the spin-down levels can be obtained from the spin-up data through a mirror reflection on the Fermi energy (which is set to $E_F = 0$).

(the corresponding curves for spin-down are given by a mirror reflection on the energy axis around the Fermi energy). Unlike other states, and for obvious symmetry reasons, the FM state presents asymmetric transport behaviors for the two spin orientations since it has a nonzero net magnetization. In all the other cases the symmetry of the spin distribution imposes identical transport properties for both spins. Notice the remarkable differences in conductance profiles between different magnetic states. While FM is the only metallic state, the LAFM case presents a very small gap (∼20 meV) around $E_F = 0$ eV while the PM state has two peaks of conductance at ±20 meV around the Fermi level. The AFM state presents the widest conductance gap, followed by the TAFM configuration. As we have different transport properties for each particular magnetic state, the selection of a specific electronic energy and/or GNW's magnetic state can be used as a means to switch the current between on or off conduction states in GNW-based nanodevices. Focusing on energies around 0.4 eV, for example, the impinging electron is transmitted when the GNW is in its AFM, FM (spin up channel) or PM states, while it is blocked for the LAFM and TAFM states. In the case of the FM state this selectivity can additionally involve the electronic spin. Based on energetics, switching mechanisms are expected to be practical in these systems since the PM distribution is, in general, significantly less stable in AZ-GNWs (as well as in ZA- and ZZ-GNWs), while the energy of other spin polarized states are closer to each other. Typical values for these energy barriers between different magnetic states in GNWs can be estimated by both DFT and TBU methods as illustrated in refs 18 and 25.

We now turn to the conductance properties of AZ-GNWs by further examining the behavior of a single unit cell attached to two semi-infinite A-GNR electrodes. This structure along with a number of different stable configurations for the electronic spin are depicted in Figure 3. Such distributions are similar to the magnetic states observed in the periodic case. However, in this system, the GNW cell breaks the translational symmetry of the infinite 11-A-GNR (electrode) due to the presence of the interfaces with the terminals. Furthermore, the interfaces induce significant scattering, resulting in conductance curves that no

longer display a step-like profile (Figure 2). Because of symmetry, the structure has a zero total magnetization in the AFM, LAFM, and PM configurations. This argument is no longer valid for the FM and TAFM distributions and it follows that these states present spin-dependent transport properties.

Let us now examine the possibility of tuning the transport properties by selecting different magnetic states. The periodic and the one-cell systems present the fundamental difference that the latter requires switching the magnetic state over a finite domain (since the terminals are armchair and nonmagnetic) while the former requires flipping spins over a much larger spatial extension. This is an essential practical aspect to be considered in designing GNW devices based on spin-depending transport. We also note that, unlike the periodic case, the one cell system always presents a gap (greater than 0.2 eV). This is compatible with the electrode properties since a perfect periodic 11-A-GNR electrode has a conductance gap of ~236 meV (obtained for a periodic GNR within the same method). As this band gap is an intrinsic property of the A-GNR, the conductance for the energies close to the Fermi level is always absent in the one-cell system composed of an AZ-GNW (unless the central AZ-GNW has a wide parallel sector, attached to a correspondingly wide A-GNR which presents a smaller and smaller gap as the width becomes larger[12]). Nevertheless, the dependence of the conductance gap on the magnetic state (as can be seen on the right-hand-side of Figure 2) can provide a systematic way to modify the electronic transmission probability by selecting specific spin distributions in order to suit specific nanoelectronic applications.

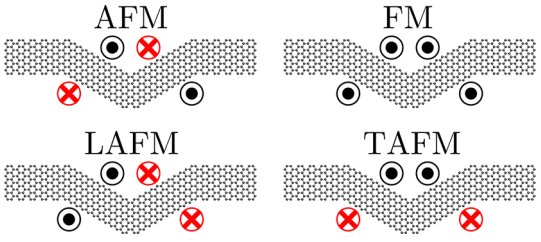

Figure 3. Schematic illustration of the four possible spin-polarized distributions for a single (11_A,6_Z) AZ-GNW cell attached to two semi-infinite 11-A-GNR electrodes. Here, black (red) circles with a dot (cross) represent majority spin up (down) for the atoms along the corresponding zigzag edges.

ZA-GNWs—Selecting Spin Current. A similar procedure as that employed above was used to study the (5_Z,13_A) structure as a representative example of the ZA-GNW class. This system, in its periodic configuration, presents a reduced set of magnetic states compared to the AZ-GNWs.[18] On the left-hand-side of Figure 4 we plot the quantum conductance for the spin-up channels in the AFM, FM, and PM states (the conductance for the spin-down levels can be obtained from the spin-up data through a mirror reflection around E_F). As expected, AFM and PM display spin degenerated curves for the conductance due to their symmetric spin distribution. The AFM state has a ~265 meV gap around the Fermi energy. Moving to the PM case, a highly localized conductance peak appears at the zero energy point which is surrounded by two conductance plateaus separated by a very small gap (~34 meV). Finally, the FM state presents a ~30 meV gap. However, in contrast with the AFM and PM cases, the gap in the FM state lies between pure spin-up and spin-down levels. It follows that the spin character of the current can be controlled by setting the impinging electron energy slightly above or below the Fermi energy.

The system made up of a ZA-GNW cell sandwiched between two semi-infinite 5-Z-GNR terminal presents a larger number of dissimilar spin distributions compared with the periodic case. This diversity comes about from the two possible spin distributions along the Z-GNR terminals for each local spin distribution from the central GNW unit cell. These different distributions are depicted in Figure 5. The labels AFM1, AFM2, FM1, and FM2 correspond to the different possible spin distributions between the top edge of the electrodes and the bottom edge of the finite-size GNW. The corresponding spin-up conductance curves

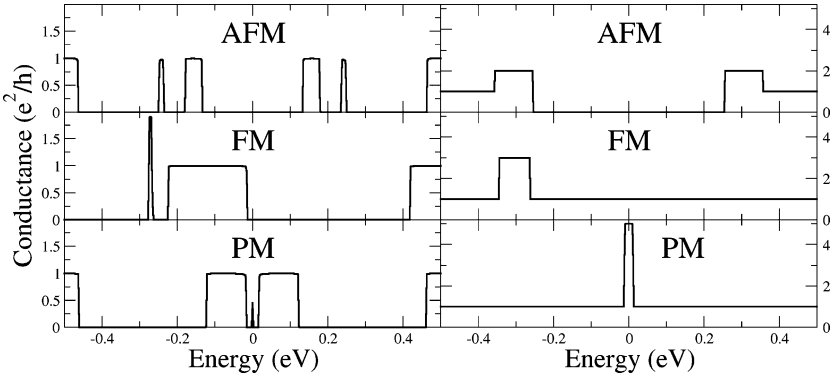

Figure 4. Quantum conductance as a function of energy for the spin-up levels in the three possible magnetic states for the periodic (5_Z,13_A) ZA-GNW structure (left) and for the periodic 5-Z-GNR (right). The corresponding curves for spin-down levels can be obtained from the spin-up results by a mirror reflection around the Fermi energy (E_F = 0).

for these one-cell systems are plotted in Figure 6 (the corresponding spin-down curves are obtained through a mirror reflection on the spin-up data around E_F). We observe that electronic transmission is substantially suppressed in the [−0.5 eV, +0.5 eV] energy range for the AFM1 case. After a gap of about 0.5 eV, the conductance slowly increases. The same behavior is observed for FM2, with the exception of the presence of conductance spikes located close to ±0.25 and ±0.35 eV. This behavior is directly related to the terminal properties since these are in their AFM state with a ∼0.5 eV conductance gap around the Fermi energy (see the right of Figure 4).

According to definitions provided in Figure 5, the AFM2 and FM1 states have Z-GNR terminals in their FM state (which is metallic - see right of Figure 4). In the FM1 case we note two broad conductance peaks (centered close to −112 and −222 meV) in the valence band for spin up (majority spin) and two symmetrically positioned peaks (112 and 222 meV) in the conduction band for spin-down electrons. This is compatible with the properties of both 5-Z-GNR terminals and the (5_Z,13_A) system. Since the periodic 5-Z-GNR system presents a constant, finite conductance in the energy range to which these peaks belong, the periodic ZA-GNW system presents 208 meV wide conductance plateaus in the same energy intervals. We observe that, around the Fermi energy, the occupied states conductance ($E < 0$) corresponds to the majority spin, while the electron−electron interaction pushes the opposite spin levels to higher energies so that the conductance for the unoccupied levels ($E > 0$) is dominated by the minority spin levels. As a result, one can imagine being able to switch the spin character of the current by selecting either the occupied or unoccupied states.

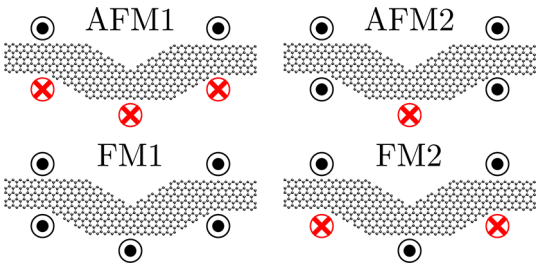

Figure 5. Four possible spin-polarized distributions for a single (5_Z,13_A) AZ-GNW cell attached to two semi-infinite 5-Z-GNR electrodes. In the plots, black (red) circles with a dot (cross) represent majority spin up (down) for the atoms along the corresponding zigzag edges.

This effect can be further understood by examining the local current distribution. In Figure 7 we show the local current plot for the spin-up states in the FM1 distribution considering that the terminals are filled according to the chemical potentials $\mu_1 = 0$ and $\mu_2 = -0.1$ eV (see eq 1 in the methods section). In this plot we highlight the direction of the intersite local currents I_{ij} by drawing black arrows when this value is at least 10% of the maximum value ($I_{max} = 0.46\ \mu A$ for this particular structure). First, let us examine the current profile for the spin-up levels. We observe that the current is spread over the valley region of the Z-GNR terminals and the central wiggle structure (i.e., where the graphene sublattices are interrupted) corresponds to a narrow funnel where the current concentrates on the inner corner of the GNW cell. It follows that chemical or physical modifications on these structures are expected to affect the transport properties specially when operated on these particular sites, making these structures potential candidates for nanosensor applications with high spatial resolution. On the other hand, the current is significantly reduced for the spin-down case (where $I_{max} = 0.047\ \mu A$) as expected from the conductance plots (Figure 6). These features for spin-up and -down states are interchanged when considering that the leads are filled according to the chemical potentials $\mu_1 = 0$ and $\mu_2 = 0.1$ eV (not shown).

Turning to the AFM2 state (which also has 5-Z-GNR terminals in their FM state) highlights the possibility of an alternate mechanism to select the spin polarization of the electronic current. In this case we still have

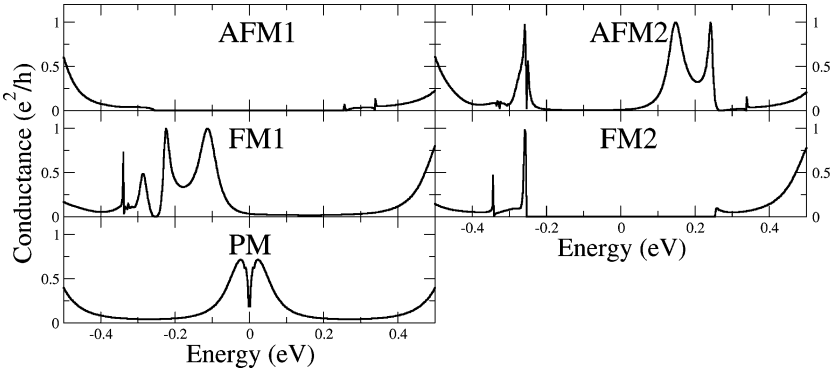

Figure 6. Quantum conductance as a function of energy for the five possible spin distributions of a single (5_Z,13_A) ZA-GNW unit cell attached to two semi-infinite 5-Z-GNR terminals (spin-up curves). Spin-down curves are obtained by a mirror reflection around the Fermi energy (set to $E_F = 0$).

two similar peaks for each spin channel, but their positions relative to the Fermi level are inverted: the conductance close to the Fermi level for occupied states is now dominated by the spin down electrons (minority spin on the Z-GNR terminals), while the conductance for the unoccupied states is dominated by spin up electrons (majority spin on the terminals). This can seem surprising, in principle, as we could expect the majority (minority) of spin electrons to be responsible for the conductance from the occupied (unoccupied) states. However, as shown below, an analysis on the density of states (DOS) explains the origin of this apparent paradox.

The DOS is shown in Figure 8. Clearly, a very large portion of the DOS below (above) E_F corresponds to the majority (minority) spin in both FM1 and AFM2. The states corresponding to the AFM2 and FM1 conductance peaks close to E_F (in Figure 6) are marked by arrows in the DOS plots from Figure 8. These particular states behave differently from most of the states close to E_F and change their position relative to the Fermi energy depending on whether the system is in its FM1 or AFM2 distribution. Therefore, the conductance for states below and above the Fermi energy can be switched between spin-up and -down conduction by switching the spin polarization along the zigzag edge sector indicated by the arrows in the left of Figure 9. Finally, the PM distribution presents two symmetric conductance peaks around the Fermi level.

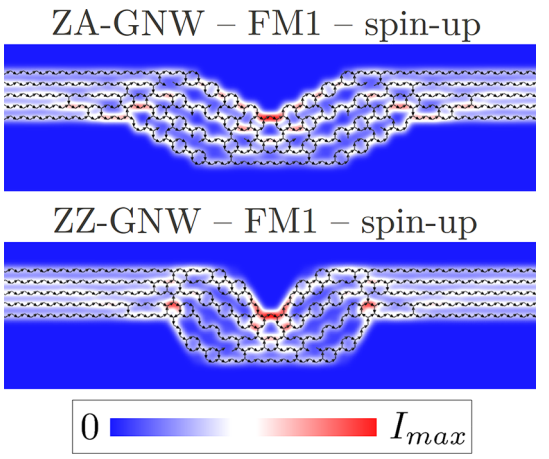

Figure 7. Local current distribution $I(x,y)$ for the one-cell (5_Z,13_A) ZA-GNW and (5_Z,8_Z) ZZ-GNW systems in the FM1 distribution corresponding to spin-up states. The terminals are filled according to the chemical potentials $\mu_1 = 0$ and $\mu_2 = -0.1$ eV for the ZA structure and $\mu_{1/2} = \pm 0.05$ eV for the ZZ case. The maximum intersite local current value for the plot is $I_{max} = 0.46\ \mu A$ ($I_{max} = 1.84\ \mu A$) for the ZA (ZZ) system. Arrows are used to highlight the direction of the intersite local currents I_{ij} when this value reaches at least 10% of the maximum value I_{max}.

ZZ-GNWs—Turning the Current ON and OFF. We selected the (5_Z,8_Z) system to study the ZZ-GNW class. ZZ-GNWs can assume a number of magnetic states: two antiferromagnetic states (AFM and transverse-AFM, TAFM), one ferromagnetic state (FM), a longitudinal ferrimagnetic state (LFiM), and the trivial nonmagnetic state (PM).[18] In this system, no significant spin polarization is developed along its short oblique edges so that the AFM and TAFM distributions are indistinguishable, similar to the FM and LFiM distributions. In the left of Figure 10 we plot the conductance as a function of energy (corresponding to spin-up states) for the periodic (5_Z,8_Z) system in the AFM, FM, and PM states (spin-down curves are obtained by a mirror operation around E_F). The AFM state presents a 338 meV conductance gap around the Fermi energy, while the PM case is metallic (nonzero conductance at E_F). Both AFM and PM states have degenerated spin-up and -down conductance spectra as a consequence of the symmetry of their spin distributions. Finally, the FM state presents a small gap around $E_F = 0$ separating states with spin-up and -down. This is similar to what was observed in the periodic (5_Z,13_A) structure in its FM state, but with one noteworthy difference: the conducting levels below (above) the Fermi energy correspond to the minority (majority) spin. This behavior is opposite to the (5_Z,13_A) case where the conductance plateau just below E_F for the FM state corresponds to the majority spin.

Although the particular ZZ-GNW system selected here does not present the five different possible spin distributions within a single unit cell as most

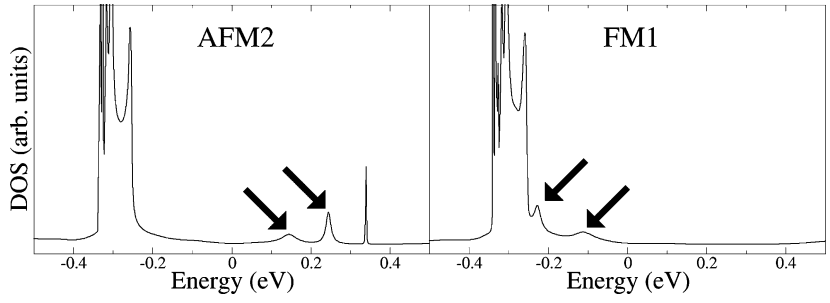

Figure 8. Spin-up DOS as a function of energy for the AFM2 and FM1 spin distributions for a single (5_Z,13_A) ZA-GNW unit cell attached to two semi-infinite 5-Z-GNR terminals calculated using the algorithm from ref 31. Spin-down curves can be obtained from the spin-up data by mirror reflections along the energy axis around the Fermi energy ($E_F = 0$).

ZZ-GNWs,[25] it is well-suited for comparison with the ZA-GNW case presented in the previous section. The one-cell system for this ZZ-GNW has five possibilities for the spin distribution which are analogous to the five corresponding distributions on the ZA-GNW one-cell system (Figure 5). When analyzing the data of the one-cell system (spin-up curves on the right of Figure 10; spin-down curves are identical to spin-up curves after a mirror reflection around E_F), we observe that both AFM1 and FM2 states have a ~555 meV conductance gap around E_F. In the AFM1 case we note two asymmetric conductance peaks out of which the sharpest is suppressed in the FM1 state, suggesting that switching between AFM1 and FM2 can be used to turn the conductance ON and OFF for these particular values of energy.

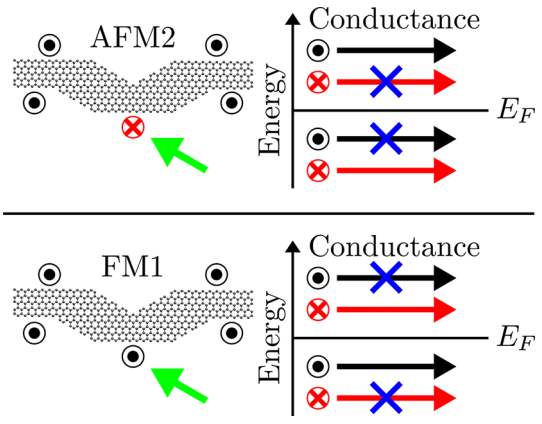

Figure 9. Switching mechanism for the spin-up and -down conductance involving the AFM2 and FM1 states in a single (5_Z,13_A) ZA-GNW unit cell attached to two semi-infinite 5-Z-GNR terminals. Spin up (down) is represented by black (red) circles with a dot (cross).

Focusing on the FM1 state, one observes a broad conductance peak around the Fermi level which is slightly asymmetric for spin-up and -down states. When flipping the spin polarization on the zigzag edge highlighted in Figure 9 we obtain the AFM2 state, and the central broad peak is turned OFF while we preserve a number of conductance peaks on the left (right) of E_F for spin-up (-down) electrons. Another change is the appearance of two peaks on the right (left) of E_F for spin-up (-down) levels. Further insight can be obtained form the current distribution across the conductor. The current due to the nonequilibrium conditions brought about by chemical potentials $\mu_{1/2} = \pm 0.05$ eV is plotted in Figure 7 for the spin-up levels in the FM1 state (with similar behavior for the spin-down levels, not shown in Figure 7). Similar to previous discussion of the current profile, local currents I_{ij} which are at least 10% of the maximal local current (I_{max} = 1.84 μA) have their directions highlighted by arrows between the corresponding sites. Similarly to the spin-up levels in the FM1 state from the ZA structure, the spin-up FM1 current in the ZZ system is distributed mostly over the GNR valley, while it concentrates on the inner corner of the GNW cell (where the local current reaches its maximum value). Moving to the AFM2 case (not shown), the current amplitude barely reaches 0.12 μA, which is less than 10% of the maximum value from the ON, FM1 state. We see that all the changes are governed by a local modification of the orientation for the spin along the finite parallel edge from the central GNW cell. The PM states behaves similarly to the

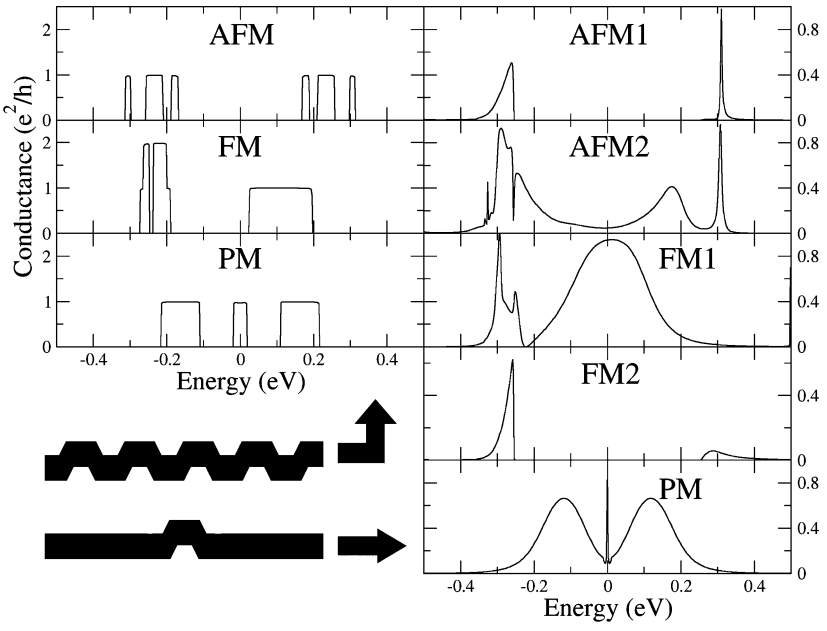

Figure 10. Quantum conductance (spin-up) as a function of energy for the three possible spin distributions in the periodic (5_Z,8_Z) ZZ-GNW structure (left) and for the other five spin-configurations in the corresponding one-cell system. Spin-down curves can be obtained from the spin-up case through a mirror reflection around the Fermi energy (E_F = 0).

ZA-GNW case, except for the presence of a sharp peak on the Fermi level.

CONCLUSIONS

In this letter we used ballistic transport formalism to demonstrate that the different magnetic states in GNWs have a profound influence on the electronic transmission. The conductance pattern in both periodic and one-cell systems are found to be tunable by selecting appropriate energy of the impinging electron in a specific magnetic state. Such features clearly indicate the possibility of using GNWs for the design of new nanoscale devices with spin-dependent properties. We showed that manipulations of the transport properties can be conducted through both localized and extended modifications of the spin distribution over the GNW systems. In light of the ever increasing experimental control in creating these structures, the realization of GNWs-based integrated nanocircuits seems to be more and more likely to occur in a near future, allowing for the development of novel nanoswitch devices and other smart spintronic systems.

METHODS

Quantum conductance of extended GNW/GNR systems was computed using a Green's function (GF) approach.[32] For the GF calculation we write the Hamiltonian in terms of a tight-binding description which includes a Hubbard model Hamiltonian (TBU) for which the occupancies for spin-up and -down states are determined self-consistently.[18,33] The TBU calculations are restricted to the π-orbitals for the graphitic structures. Despite its simplicity, this approach is known to yield accurate results, when compared to density functional theory, provided interactions up to third nearest neighbors are included.[34] We follow the parametrization from ref 34 so that we used $\gamma_1 = 3.2$ eV, $\gamma_2 = 0$ eV, and $\gamma_3 = 0.3$ eV for the first-, second-, and third-nearest neighbor hopping integrals, respectively, including a $\Delta\gamma_1 = 0.2$ eV correction to the γ_1 parameter for the edge atoms to account for the different coordination number at the borders of the system. Note that the edge atoms are saturated with hydrogens (as implicitly considered within this π-orbital model). The $U = 0.92\gamma_1$ parameter for the electronic on-site repulsion included in the Hubbard Hamiltonian is parametrized using *ab initio* calculations.[18] A detailed description of this model Hamiltonian can be found in a recent publication.[25]

In the computational packages we developed to perform these calculations, the conductor's Green's function is obtained using an efficient recursive algorithm recently proposed in the literature where the Dyson equation is repeatedly applied until no explicit matrix inversion is necessary.[31]

We can attain further qualitative insight into the profile of the charge flow by plotting the local current. The current I_{ij} between any two sites, i and j, can be calculated with the aid of the lesser GF ($G^<$) with[31,35]

$$I_{ij} = \frac{e}{h}\int_{-\infty}^{\infty} dE(t_{ij}G^<_{ji}(E) - t_{ji}G^<_{ij}(E)) \quad (1)$$

where $t_{ij} = t^*_{ji}$ is the hopping between sites i and j. In the absence of electronic correlations, $G^<$ can be directly obtained from the retarded GF (G_R) by

$$G^<(E) = G_R\Sigma^<G_R^\dagger; \quad \Sigma^< = \sum_l f_l(\Sigma_l^\dagger - \Sigma_l) \quad (2)$$

where the sum runs over all the terminals, Σ_l is the lth terminal self-energy, and f_l is the corresponding Fermi distribution used to fill the terminal states according to the chemical potential μ_l.

To ease the visualization of the local current data, we represent the local current in a real space representation:

$$I(x,y) = \sum_{i\neq j}\alpha_{ij}\langle \mathbf{r}|i\rangle\langle i|I|j\rangle\langle j|\mathbf{r}\rangle \quad (3)$$

where $\langle i|I|j\rangle = I_{ij}$ and $\langle \mathbf{r}|i\rangle = e^{-r^2}/a_{CC}^2$ with r being the distance from the point (x,y) to the position of site i. As $I_{ij} = -I_{ji}$ (see eq 1), we select only the positive values of I_{ij} by setting $\alpha_{ij} = 1$ (0) when $I_{ij} \geq 0$ ($I_{ij} < 0$).

Note that these equations are only formally correct for full nonequilibrium, self-consistent calculations. However, they remain applicable at very low-bias potential, especially for a qualitative study as that provided in Figure 7.

The self-consistent occupancies related to the Hubbard Hamiltonian were obtained using periodic boundary conditions. For the one cell systems, we included a large number of GNR unit cells on each side of the GNW cell in order to allow the extreme electrode cells to recover the properties of the bulk. For the ZA and ZZ cases we used 35 Z-GNR unit cells (corresponding to a length of 86.1 Å) on each side of the GNW cell (70 Z-GNR cells in total). In the other AZ case we used 20 A-GNR unit cells (i.e., a 85.2 Å length) on each side of the central GNW cell (40 cells in total). These large buffer sections made the calculations more challenging but were found to lead to a well-converged solution amenable to be recast in a setup relevant to a transport calculation where the GNR electrodes are modeled as semi-infinite.

Conflict of Interest: The authors declare no competing financial interest.

Acknowledgment. ECG acknowledges the Brazilian agencies CAPES for the sandwich program fellowship (process 0327-10-7) and CNPq (process 140887/2008-3). E.C.S. was supported in part by PHASE, an EFRC funded by the US-DOE under Award Number DE-SC0001087. V.M. is supported by New York State under NYSTAR contract C080117. All the calculations were performed on resources from the Computational Center for Nanotechnology Innovation at RPI. The authors thank Prof. Antônio Gomes Souza Filho and M.S. Liangbo Liang for valuable discussions.

REFERENCES AND NOTES

1. Novoselov, K.; Geim, A.; Morozov, S.; Jiang, D.; Zhang, Y.; Dubonos, S.; Grigorieva, I.; Firsov, A. Electric Field Effect in Atomically Thin Carbon Films. *Science* **2004**, *306*, 666–669.
2. Palma, C.-A.; Samori, P. Blueprinting Macromolecular Electronics. *Nat. Chem.* **2011**, *3*, 431–436.
3. Van Noorden, R. The Trials of New Carbon. *Nature* **2011**, *469*, 14–16.
4. Cruz-Silva, E.; Barnett, Z. M.; Sumpter, B. G.; Meunier, V. Structural, Magnetic, and Transport Properties of Substitutionally Doped Graphene Nanoribbons from First Principles. *Phys. Rev. B* **2011**, *83*, 155445.
5. Amorim, R. G.; Fazzio, A.; Antonelli, A.; Novaes, F. D.; da Silva, A. J. R. Divacancies in Graphene and Carbon Nanotubes. *Nano Lett.* **2007**, *7*, 2459–2462.
6. Jia, X.; Campos-Delgado, J.; Terrones, M.; Meunier, V.; Dresselhaus, M. S. Graphene Edges: A Review of Their Fabrication and Characterization. *Nanoscale* **2011**, *3*, 86–95.
7. Chang, Y. C.; Haas, S. Defect-Induced Resonances and Magnetic Patterns in Graphene. *Phys. Rev. B* **2011**, *83*, 085406.
8. Pedersen, T. G.; Flindt, C.; Pedersen, J.; Mortensen, N. A.; Jauho, A.-P.; Pedersen, K. Graphene Antidot Lattices: Designed Defects and Spin Qubits. *Phys. Rev. Lett.* **2008**, *100*, 136804.
9. Lahiri, J.; Lin, Y.; Bozkurt, P.; Oleynik, I. I.; Batzill, M. An Extended Defect in Graphene as a Metallic Wire. *Nat. Nanotechnol.* **2010**, *5*, 326–329.

10. Botello-Mendez, A. R.; Declerck, X.; Terrones, M.; Terrones, H.; Charlier, J. C. One-Dimensional Extended Lines of Divacancy Defects in Graphene. *Nanoscale* **2011**, *3*, 2868–2872.
11. Son, Y.-W.; Cohen, M. L.; Louie, S. G. Half-Metallic Graphene Nanoribbons. *Nature* **2006**, *444*, 347–349.
12. Son, Y.-W.; Cohen, M. L.; Louie, S. G. Energy Gaps in Graphene Nanoribbons. *Phys. Rev. Lett.* **2006**, *97*, 216803.
13. Pisani, L.; Chan, J. A.; Montanari, B.; Harrison, N. M. Electronic Structure and Magnetic Properties of Graphitic Ribbons. *Phys. Rev. B* **2007**, *75*, 064418.
14. Fernández-Rossier, J.; Palacios, J. J. Magnetism in Graphene Nanoislands. *Phys. Rev. Lett.* **2007**, *99*, 177204.
15. Jiang, D.; Dai, S. Circumacenes *versus* Periacenes: HOMO–LUMO Gap and Transition from Nonmagnetic to Magnetic Ground State with Size. *Chem. Phys. Lett.* **2008**, *466*, 72–75.
16. Hod, O.; Barone, V.; Scuseria, G. E. Half-metallic Graphene Nanodots: A Comprehensive First-Principles Theoretical Study. *Phys. Rev. B* **2008**, *77*, 035411.
17. Ma, Z.; Sheng, W. A Spin-Valve Device Based on Dumbbell-Shaped Graphene Nanoislands. *App. Phys. Lett.* **2011**, *99*, 083101.
18. Girão, E. C.; Liang, L.; Cruz-Silva, E.; Souza Filho, A. G.; Meunier, V. Emergence of Atypical Properties in Assembled Graphene Nanoribbons. *Phys. Rev. Lett.* **2011**, *107*, 135501.
19. Saffarzadeh, A.; Farghadan, R. A Spin-Filter Device Based on Armchair Graphene Nanoribbons. *App. Phys. Lett.* **2011**, *98*, 023106.
20. Sevincli, H.; Topsakal, M.; Ciraci, S. Superlattice Structures of Graphene-Based Armchair Nanoribbons. *Phys. Rev. B* **2008**, *78*, 245402.
21. Topsakal, M.; Sevincli, H.; Ciraci, S. Spin Confinement in the Superlattices of Graphene Ribbons. *App. Phys. Lett.* **2008**, *92*, 173118.
22. Muñoz Rojas, F.; Fernández-Rossier, J.; Palacios, J. J. Giant Magnetoresistance in Ultrasmall Graphene Based Devices. *Phys. Rev. Lett.* **2009**, *102*, 136810.
23. Botello-Mendez, A. R.; Cruz-Silva, E.; Romo-Herrera, J. M.; Lopez-Urias, F.; Terrones, M.; Sumpter, B. G.; Terrones, H.; Charlier, J. C.; Meunier, V. Quantum Transport in Graphene Nanonetworks. *Nano Lett.* **2011**, *11*, 3058–3064.
24. Cai, J.; Ruffieux, P.; Jaafar, R.; Bieri, M.; Braun, T.; Blankenburg, S.; Muoth, M.; Seitsonen, A. P.; Saleh, M.; Feng, X.; *et al.* Atomically Precise Bottom-up Fabrication of Graphene Nanoribbons. *Nature* **2010**, *466*, 470–473.
25. Girão, E. C.; Cruz-Silva, E.; Liang, L.; Souza Filho, A. G.; Meunier, V. Structural and Electronic Properties of Carbon Nanowiggles. *Phys. Rev. B* **2012**, *85*, 235431.
26. Chen, Y.; Jayasekera, T.; Calzolari, A.; Kim, K. W.; Nardelli, M. B. Thermoelectric Properties of Graphene Nanoribbons, Junctions and Superlattices. *J. Phys.-Condens. Matter* **2010**, *22*, 372202.
27. Huang, W.; Wang, J.-S.; Liang, G. Theoretical Study on Thermoelectric Properties of Kinked Graphene Nanoribbons. *Phys. Rev. B* **2011**, *84*, 045410.
28. Datta, S. *Quantum Transport: Atom to Transistor*; Cambridge University Press: Cambridge, UK, 2005.
29. Landauer, R. Conductance Determined by Transmission Probes and Quantized Constriction Resistance. *J. of Phys. Condens. Matter* **1989**, *1*, 8099–8110.
30. Fisher, D. S.; Lee, P. A. Relation between Conductivity and Transmission Matrix. *Phys. Rev. B* **1981**, *23*, 6851–6854.
31. Kazymyrenko, K.; Waintal, X. Knitting Algorithm for Calculating Green Functions in Quantum Systems. *Phys. Rev. B* **2008**, *77*, 115119.
32. Nardelli, M. B. Electronic Transport in Extended Systems: Application to Carbon Nanotubes. *Phys. Rev. B* **1999**, *60*, 7828–7833.
33. Yazyev, O. V. Emergence of Magnetism in Graphene Materials and Nanostructures. *Rep. Prog. Phys.* **2010**, *73*, 056501.
34. Gunlycke, D.; White, C. T. Tight-Binding Energy Dispersions of Armchair-Edge Graphene Nanostrips. *Phys. Rev. B* **2008**, *77*, 115116.
35. Caroli, C.; Combesco, R.; Nozieres, P.; Saintjam, D. Direct Calculation of Tunneling Current. *J. Phys. C: Solid State Phys.* **1971**, *4*, 916.